



HAL
open science

Sensitivity analysis of the second and third-order velocity structure functions to the Reynolds number in decaying and forced isotropic turbulence using the EDQNM model

M. Meldi, L. Djenidi, R.A. Antonia

► To cite this version:

M. Meldi, L. Djenidi, R.A. Antonia. Sensitivity analysis of the second and third-order velocity structure functions to the Reynolds number in decaying and forced isotropic turbulence using the EDQNM model. *European Journal of Mechanics - B/Fluids*, 2021, 88, pp.229-242. 10.1016/j.euromechflu.2021.04.003 . hal-03266954

HAL Id: hal-03266954

<https://hal.science/hal-03266954>

Submitted on 9 May 2023

HAL is a multi-disciplinary open access archive for the deposit and dissemination of scientific research documents, whether they are published or not. The documents may come from teaching and research institutions in France or abroad, or from public or private research centers.

L'archive ouverte pluridisciplinaire **HAL**, est destinée au dépôt et à la diffusion de documents scientifiques de niveau recherche, publiés ou non, émanant des établissements d'enseignement et de recherche français ou étrangers, des laboratoires publics ou privés.



Distributed under a Creative Commons Attribution - NonCommercial 4.0 International License

Sensitivity analysis of the second and third-order velocity structure functions to the Reynolds number in decaying and forced isotropic turbulence using the EDQNM model

M. Meldi^{*a}, L. Djenidi¹, R. A. Antonia¹

^a*Institut Pprime, Department of Fluid Flow, Heat Transfer and Combustion, CNRS - ENSMA - Université de Poitiers, UPR 3346, SP2MI - Téléport, 211 Bd. Marie et Pierre Curie, B.P. 30179 F86962 Futuroscope Chasseneuil Cedex, France*

^b*Discipline of Mechanical Engineering, School of Engineering, University of Newcastle, Newcastle, 2308 NSW, Australia*

Abstract

Numerical calculations based on a recent version of the eddy-damped quasi-normal model (EDQNM-LMFA) are carried out for homogeneous isotropic turbulence (HIT) with the aim of investigating the dependency on the Reynolds number of second and third order velocity structure functions. The quantities investigated include the energy spectrum E , the non-linear energy transfer T as well as the second (S_2) and third (S_3) order moments of the longitudinal velocity increment. Both free decaying HIT and (steady state) forced HIT are considered. The analysis of the structure functions for $Re_\lambda \in [50, 10^6]$ indicates that, regardless of whether one considers decaying or forced HIT, the large scales affect S_2 and S_3 in the scaling range. In that range, forcing affects S_2 and S_3 differently. For forced HIT, $S_2/(\bar{\epsilon}r)^{2/3}$ exhibits a distinct "bump" near the upper end of the scaling range while no such bump is seen for $S_3/(\bar{\epsilon}r)$. The latter quantity remains approximately constant for values of r which extend to the scale corresponding to the forcing. For decaying HIT, there is no discernible bump in either $S_2/(\bar{\epsilon}r)^{2/3}$ or $S_3/(\bar{\epsilon}r)$. The slope of S_3 in the scaling range approaches the theoretical value of 1, when Re_λ is sufficiently large. However, at similar Re_λ , the slope of S_2 has not yet reached a constant for either decaying or forced HIT.

Keywords: HIT, EDQNM, turbulence modelling

^{*}Corresponding author, marcello.meldi@ensma.fr

1. Introduction

The study of homogeneous isotropic turbulence (HIT) using two-point statistics has proven to be quite fruitful, particularly as a result of the major contribution by Von Karman & Howarth [1] who developed a transport equation for the two-point longitudinal velocity correlation $f(r, t)$ defined as $f(r, t) = \overline{u(\mathbf{x}, t)u(\mathbf{x} + r, t)}/U^2(\mathbf{x}, t)$, where \mathbf{x} is a spatial position, r is the magnitude of the longitudinal separation \mathbf{r} and $U^2 = \frac{2}{3}\mathcal{K}(t)$ ($\mathcal{K}(t)$ is the turbulent kinetic energy); the over-bar represents an ensemble average. Here $u(\mathbf{x}, t)$ is the longitudinal velocity component of the velocity \mathbf{u} i.e. $u(\mathbf{x}, t) = \mathbf{u}(\mathbf{x}, t) \cdot \mathbf{r}/r$. The transport equation for $f(r, t)$, now referred to as the Karman–Howarth (hereafter denoted KH) equation and written below

$$\frac{\partial f(r, t)U^2(t)}{\partial t} - 2U^3(t) \left(\frac{\partial h(r, t)}{\partial r} + \frac{4}{r}h(r, t) \right) = 2\nu U^2(t) \left(\frac{\partial^2 f(r, t)}{\partial r^2} + \frac{4}{r} \frac{\partial f(r, t)}{\partial r} \right) + W_f \quad (1)$$

where $h(r, t) = \overline{u(\mathbf{x}, t)u(\mathbf{x}, t)u(\mathbf{x} + r, t)}/(U^2(\mathbf{x}, t))^{3/2}$ is the third order velocity correlation, marked a milestone for the theory of HIT. The term W_f represents the correlation between a volume source term (forcing) and the velocity fluctuation in the Navier–Stokes equations. This term is zero for decaying HIT. Equally useful two-point statistical quantities for the theory of HIT are the so-called longitudinal velocity structure functions defined as

$$S_n(r, t) = \overline{[u(\mathbf{x} + r, t) - u(\mathbf{x}, t)]^n} = \overline{(\delta u)^n}. \quad (2)$$

where $\delta u = u(x + r) - u(x)$ is the velocity increment. Of particular interest are the 2nd and 3rd order structure functions. The former is related to $f(r)$ as follows

$$S_2(r, t) = \frac{2}{3}\mathcal{K}(1 - f(r, t)), \quad (3)$$

Its transport equation, which can be derived from the Navier-Stokes equations in similar fashion to equation (1), can be expressed as

$$\frac{2}{3} \frac{\partial \mathcal{K}}{\partial t}(t) = -\frac{2}{3}\bar{\varepsilon} = \frac{1}{2} \frac{\partial S_2}{\partial t} + \frac{1}{6r^4} \frac{\partial r^4 S_3}{\partial r} - \frac{\nu}{r^4} \frac{\partial}{\partial r} \left(r^4 \frac{\partial S_2}{\partial r} \right) + W_S \quad (4)$$

where $\bar{\varepsilon}$ is the ensemble average of the instantaneous turbulent energy dissipation rate and W_S is the spatial counterpart of W_f . Assuming an infinitely large Reynolds number and considering that turbulence at small-scales is in a statistically steady state, allowed Kolmogorov [2] to drop the first term on

the right side of (4) in his *K41* theory. After integration with respect to r , one obtains:

$$S_3(r, t) = -\frac{4}{5}\bar{\varepsilon}r + 6\nu\frac{\partial}{\partial r}S_2(r, t) + Z. \quad (5)$$

After neglecting the second term on the right of (5) and Z , which represents the effects of the energy injected at large scales and, for convenience, will be denoted loosely as "turbulence production" hereafter, eq. (5) reduces to the 4/5 law [2]

$$S_3(r, t) = -\frac{4}{5}\bar{\varepsilon}r. \quad (6)$$

The dropping of $\frac{\partial S_2}{\partial t}$, *i.e.* the first term on the right side of (4), is critical for the establishment of (5). This term reflects the contribution of the large scales to all scales of motion and if reinstated in (5) yields [3, 4]

$$S_3(r, t) = -\frac{4}{5}\bar{\varepsilon}r + 6\nu\frac{\partial}{\partial r}S_2(r, t) - \frac{3}{r^4}\int_0^r s^4\frac{\partial S_2}{\partial t}ds + Z \quad (7)$$

10 In decaying HIT, $Z = 0$ and $\partial S_2/\partial t \neq 0$, which reflects the statistical time
 11 evolution of HIT features such as the energy spectrum $E(k, t)$ (k is the wave
 12 number space of the spectral transform). However, $\partial S_2/\partial t \neq 0$ can also be
 13 associated with the non-homogeneity either in time (*e.g.*, 3D periodic box
 14 turbulence) or in space (*e.g.* grid turbulence). In direct numerical simula-
 15 tions (DNS) of a forced steady state 3D periodic turbulence, $\partial S_2/\partial t = 0$ and
 16 the term Z represents the imposed forcing at given (mainly large) scales.
 17 Notice that Z and the third term on the right side of (7), which may also be
 18 considered as a some sort of forcing caused by the large scales, represent a
 19 cumulative effect suggesting that the impact of different forms of forcing on
 20 the transport of $S_2(r)$ at a given scale may be felt differently. This would be
 21 consistent with the results of Thiesset et al. [5] and Antonia et al. [6], who
 22 showed that, at finite Reynolds numbers, the balance between the longitu-
 23 dinal velocity derivative and the destruction coefficient of enstrophy in the
 24 transport equation for $\bar{\varepsilon}$ depends on the type of large-scale forcing and thus
 25 differs from flow to flow. Further, Tang et al. [7] showed that the impact of
 26 the forcing in various turbulent flows at small and moderate Re_λ , the Tay-
 27 lor microscale Reynolds number, felt at scales of the order of λ , the Taylor
 28 microscale, depends on the types of flow under consideration. For example,
 29 they found that for a given Re_λ this impact is largest on the centreline of a
 30 fully developed channel flow but smallest for stationary forced periodic box
 31 turbulence. For decaying-type flows, the strength of this impact lies between
 32 the previous two cases. These observations corroborate the results of Qian
 33 [8], Antonia & Burattini [9] and Tchoufag et al. [10] who showed that the

34 magnitude of the maximum of $C_3 = -S_3/(\bar{\epsilon}r)$ is affected differently in forced
 35 and decaying turbulent flows; for a fixed Re_λ , the maximum is larger for
 36 forced turbulence than decaying turbulence. Tchoufag et al. [10] observed
 37 that $C_3 \approx 4/5$ for $Re_\lambda \geq 10^3$ in forced turbulence and argued that Re_λ should
 38 be larger than about 10^6 before the same maximum is observed in both types
 39 of turbulence. These observations and results illustrate the impact of the last
 40 term on the right side of (7). They further indicate that this impact is not
 41 only flow dependent but also Reynolds number dependent for a given flow
 42 when the Reynolds number is finite.

43 As noted in [11], Eq. 6 has yet to be verified convincingly on the basis
 44 of either experimental or DNS data. The expectation is that Eq. 6 is more
 45 likely to be verified when forcing is applied. Indeed, the maximum value of
 46 $4/5$ can be reached in a periodic box (e.g. the DNS data of Iyer et al. (2020)
 47 [12] at $Re_\lambda \approx 1300$). It is clear however that a plateau for $S_3/(\bar{\epsilon}r)$ has yet to
 48 be established over a range of scales when $\eta \ll r \ll L$. It is equally unclear
 49 that S_2 exhibits an unambiguous power-law behaviour in this range. It is
 50 therefore imperative to significantly extend the magnitude of Re_λ in order to
 51 ascertain if S_2 can, like S_3 , exhibit a power-law behaviour when $\eta \ll r \ll L$.

52 In the present work, the evolution with Re_λ of several second and third-
 53 order statistical moments of HIT are investigated. The physical quantities in-
 54 clude the energy spectrum E , the non-linear energy transfer T and the struc-
 55 ture functions $S_2(r)$, $S_3(r)$. The evolution of the velocity increment skewness
 56 $S(r) = S_3(r)/S_2^{3/2}$ is also considered. The analysis is performed with calcu-
 57 lations based on the eddy-damped quasi-normal model (EDQNM). In particu-
 58 lar, the EDQNM-LMFA model is employed [13]. The EDQNM model has
 59 been extensively used in the open literature to perform investigations of en-
 60 ergy spectra, non-linear energy transfer and second and third order structure
 61 functions (see, among the others, references [14, 15, 16, 17, 18, 19, 20]). The
 62 novelty aspects of the present work are i) the investigation of the sensitivity
 63 of HIT to finite Reynolds number effects, over a Reynolds number interval
 64 of almost four decades and ii) a comprehensive comparison of EDQNM data
 65 with previously published experimental / DNS data for both decaying and
 66 forced turbulence. (i) & (ii) allow us to focus on the important difference
 67 in behavior of second and third-order structure functions, between decaying
 68 and forced HIT, as Re_λ is increased significantly beyond values that are cur-
 69 rently possible either in experiment or DNS. The use of the EDQNM model
 70 seems appropriate for this purpose given that the approaches of Qian [8]
 71 and Antonia & Burattini [9] essentially assume S_2 in order to calculate S_3 ,
 72 while the EDQNM obtains S_2 from the calculation of E and T . Since no
 73 intermittency phenomenology is introduced in the constitutive hypotheses

74 of the EDQNM, the simulation captures only the Reynolds number depen-
75 dence and the effect of the production mechanisms on the physical quantities
76 investigated, with the expectation that FRN effects identified via EDQNM
77 are at least comparable to those described by the Navier-Stokes equations.
78 If so, these findings can provide insight for the analysis of results obtained
79 with more powerful numerical tools, such as DNS. As previously introduced,
80 an extensive comparison of EDQNM-LMFA results with experimental and
81 DNS data is also performed. The comparison shows that there is adequate
82 agreement for low to moderate Reynolds numbers. Thus, one can reasonably
83 expect that EDQNM data for much higher Reynolds numbers (the maxi-
84 mum value of Re_λ in the present study is 10^6) can provide an estimation of
85 the sensitivity of the turbulence to FRN effects. It will also be shown that
86 results obtained via the EDQNM-LMFA for high Reynolds number are in
87 agreement with those, based on an empirical model for S_2 , by Antonia et al.
88 [11]. Three main sets of EDQNM-LMFA calculations are performed, one for
89 freely decaying HIT and the other two for statistically steady forced HIT,
90 using different forcing terms.

91 The paper is structured as follows. The EDQNM model is described in
92 general terms in Section 2; the distribution of the forcing term F , representing
93 production mechanisms in the spectral space, is also discussed in this Section.
94 Section 3 contains a comprehensive discussion of the results. Conclusions are
95 given in Section 4. Specific features of the adopted EDQNM model are given
96 in more detail in the Appendix A.

97 2. The EDQNM model

The EDQNM model [21, 22, 23] is briefly described in this section, while
an extended discussion is provided in the Appendix A. The EDQNM is a tur-
bulence closure in spectral space and it relies on the numerical discretization
of the Lin equation:

$$\frac{\partial E(k, t)}{\partial t} + 2\nu k^2 E(k, t) = T(k, t) + F(k, t) \quad (8)$$

98 where $T(k, t)$ is the non-linear energy transfer due to triadic interactions and
99 F represents the spectral transform of production mechanisms. The EDQNM
100 closure is used to estimate $T(k, t)$ via the calculated value of $E(k, t)$ and an
101 eddy-damping term. The limitations of this model include the fact that inter-
102 mittency effects are not taken into account and only second and third-order
103 velocity structure functions can be directly calculated. The model version
104 used to perform the present analysis is the EDQNM-LMFA proposed by Bos

105 & Bertoglio [24]. The main difference between this model and the classi-
 106 cal EDQNM proposal is that a single-time closure is used to determine the
 107 eddy damping model used to estimate $T(k, t)$. This closure does not rely on
 108 heuristic constants to determine the intensity of the damping term. Instead,
 109 it is calculated within the EDQNM closure resolving an evolution equation
 110 for the velocity-displacement cross-correlation spectrum \mathcal{F}_{CC} , which is ob-
 111 tained using the formalism proposed in the Direct Interaction Approximation
 112 (DIA) theory [25]. More details about the implementation are provided in
 113 the Appendix A. For convenience, the EDQNM-LMFA model will simply
 114 be referred to as EDQNM. Physical quantities, such as the turbulent kinetic
 115 energy $\mathcal{K}(t)$ or the velocity derivative skewness $S(t)$ are derived via manipula-
 116 tion / integration of $E(k, t)$ and $T(k, t)$. In the present analysis, calculations
 117 are performed for both freely decaying HIT (i.e. $F(k, t) = 0$) and statistically
 118 steady forced turbulence ($F(k, t) = F(k)$).

Several proposals for the forcing distribution were investigated for the
 case of statistically steady forced turbulence. However, forced HIT results
 are here restricted to two forcing schemes. These two schemes were cho-
 sen according to their different distribution (local or global) in the spectral
 space. In addition, both forcing terms comply well with the very large scale
 requirements imposed by the adaptive spectral mesh strategy employed in
 the calculations [26] which will be described in the following. The first scheme
 is a single wavenumber forcing:

$$F(k) = \begin{cases} \gamma_F \cdot \bar{\varepsilon}(0) & \text{if } k = k_L(0) \\ 0 & \text{if } k \neq k_L(0) \end{cases} \quad (9)$$

119 where γ_F is a positive scalar.

The second forcing scheme employed is derived in order to obtain con-
 servation of the large-scale features i.e. $\partial E(k, t)/\partial t = 0$ for $k < k_L$, where
 $k_L(t) = L^{-1}(t)$ is the wave number associated with the integral length scale
 L . Artificial damping is applied at large wavenumbers viz.

$$F(k) = \begin{cases} 2\nu k^2 E(k) - T(k) & \text{if } k \leq k_L(0) \\ (2\nu k^2 E(k) - T(k)) \cdot r_F^{-k/k_L(0)} & \text{if } k > k_L(0) \end{cases} \quad (10)$$

120 The parameter $r_F = 1.1$ has been set to obtain a bump between the
 121 integral length scale region and the scaling range. This feature has been
 122 observed in several experimental and numerical analyses reported in the lit-
 123 erature [27, 28, 29].

Initial conditions are imposed using an energy spectrum functional form
 suggested by Pope [30] and Meyers & Meneveau [31]:

$$E_I(k) = C_K \bar{\varepsilon}^{2/3} k^{-5/3} f_L(kL) f_\eta(k\eta) \quad (11)$$

with

$$f_L(kL) = \left(\frac{kL}{[(kL)^{1.5} + c_L]^{1/1.5}} \right)^{5/3+\sigma}, \quad f_\eta(k\eta) = \exp(-\beta([(k\eta)^4 + c_\eta^4]^{1/4} - c_\eta)) \quad (12)$$

124 where $C_K \in [1.4, 1.6]$ is the Kolmogorov constant, L is the integral length
 125 scale and η is the Kolmogorov length scale. The free coefficients have been
 126 set to $c_\eta = 0.4$, $\beta = 5.3$; c_L has been chosen in order to obtain $L(0) = 1$.
 127 Calculations are performed by fixing an initial value ($= 2$) of the parameter σ .
 128 This parameter controls the shape of the energy spectrum at large scales, and
 129 the value chosen corresponds to the well known case of Saffman turbulence.
 130 Early tests choosing a value of $\sigma = 4$ (Batchelor turbulence) showed that the
 131 EDQNM prediction of S_2 and S_3 is not sensitive to the parameter σ . The
 132 initial Reynolds number has been set to $Re_\lambda = 10^6$ for the free decay case and
 133 to $Re_\lambda \in [50, 10^6]$ for the forced cases. The initial transient regime in free
 134 HIT decay is governed by the features of the functional form prescribed for
 135 $t = 0$. An increase of the Reynolds number is observed up to $Re_\lambda \approx 2 \times 10^6$
 136 for $t \approx t_0$, where $t_0 = \mathcal{K}(0)/\bar{\varepsilon}(0)$ is the initial turnover time. After this first
 137 phase, the statistics progressively lose memory of the initial condition and a
 138 classical power law decay is observed [32, 17]. For the present analysis, data
 139 are sampled in the range $10^6 \geq Re_\lambda \geq 50$. For the forced simulations, $E(k)$
 140 will converge towards a forced solution from the initially prescribed functional
 141 form $E_I(k)$. The statistically steady solution is clearly governed by the shape
 142 of the forcing term F . Finally, calculations are performed using an adaptive
 143 spectral mesh strategy [26] which conserves the large-scale resolution for the
 144 free decay case. The condition $k_L(t)/k_{min}(t) = 10^3$ has been imposed, where
 145 k_{min} is the smallest resolved mode. This choice allows confinement effects to
 146 be excluded.

147 The present study focuses on the prediction of the energy spectrum E , the
 148 non-linear energy transfer T and the structure functions S_2 and S_3 . These
 149 quantities are connected via the following integral relations [33, 23]:

$$S_2(r, t) = \int_0^{+\infty} 4 E(k, t) \left[\frac{1}{3} - \frac{\sin(kr) - (kr) \cos(kr)}{(kr)^3} \right] dk \quad (13)$$

$$S_3(r, t) = \int_0^{+\infty} 12 T(k, t) \frac{3(\sin(kr) - (kr) \cos(kr)) - (kr)^2 \sin(kr)}{(kr)^5} dk \quad (14)$$

150 using the EDQNM prediction for $E(k, t)$ and $T(k, t)$.

151 The spectra calculated using the EDQNM may exhibit remarkable differ-
 152 ences. First, a visualization of the energy spectrum E and of the multiscale
 153 forcing term F in Equation 10 is shown in Figure 1 (a)-(b). One can see

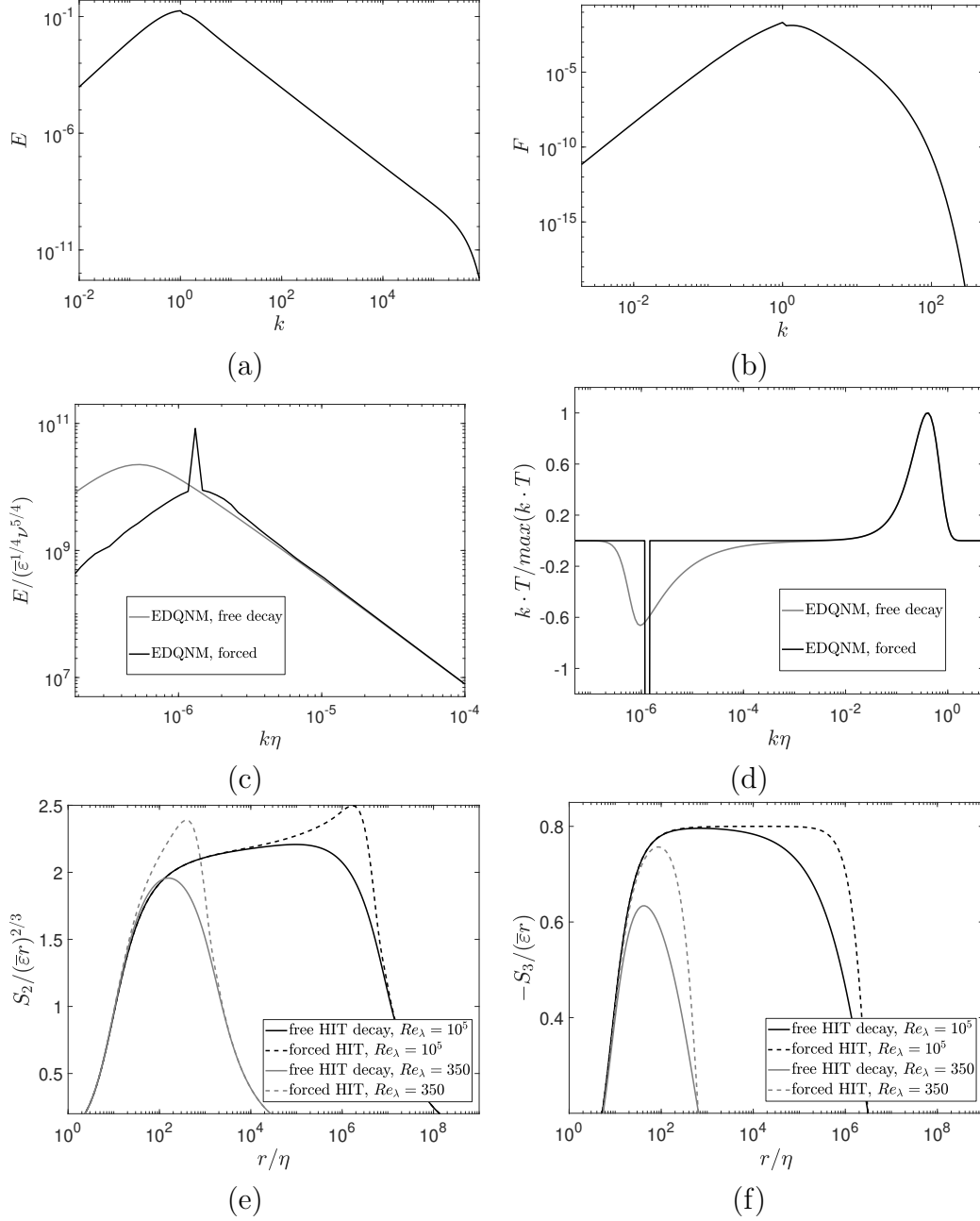


Figure 1: (a) Energy spectrum E and (b) forcing F for the case of statistically steady forced HIT using the forcing in Equation 10 for $Re_\lambda \approx 10^5$. (c) Normalized energy spectrum E and (d) non-linear energy transfer T for the cases of decaying HIT and statistically steady forced HIT (equation 9) for $Re_\lambda \approx 10^5$. (e) Second-order velocity structure function and (f) third-order velocity structure function for free decaying HIT and forced HIT.

154 the bump in the energy spectrum for $k = k_L(0) = 1$. The free decay case
 155 and the other forcing scheme (equation 9) are instead shown in Figure 1 (c)-
 156 (f). The single wavenumber distribution for F is responsible for the sharp
 157 increase in the energy spectrum $E(k)$ near the peak, as shown in figure
 158 1(c). Comparison of the non-linear energy transfer in figure 1(d) indicates
 159 that, for similar Re_λ , the free decay case exhibits a shorter scaling range.
 160 The results for the forced case show an almost perfect plateau just outside
 161 the energy production region. The analysis of the compensated third-order
 162 velocity structure function $-S_3/(\bar{\varepsilon}r)$ in figure 1 (f) provides similar informa-
 163 tion. This behaviour is intimately connected with the triadic interactions
 164 associated with very energetic modes, as discussed by Meldi & Sagaut [34].
 165 Because of the connection between T and S_3 in equation (14), this mecha-
 166 nism is also responsible for the emergence of a clearer plateau at moderate
 167 Re_λ for the third-order structure function in the case of forced HIT. Also,
 168 results from every EDQNM calculation in figure 1 (e)-(f) collapse at the small
 169 scales, indicating that the large scale behaviour does not influence the dy-
 170 namics of the small scales. In addition, all the computed spectra exhibit a
 171 power-law range proportional to k^{n_E} , $n_E \approx -5/3$ in the inertial region, once
 172 the Reynolds number is high enough. This is shown in figure 2 with the local
 173 calculation via polynomial fitting of the relation $E \propto k^{n_E}$ for the free decay
 174 case. For the highest Reynolds number considered, $Re_\lambda = 10^6$, the averaged
 175 deviation of the power law exponent within the scaling range from the K41
 176 behaviour is $\overline{n_E} + 5/3 = 5 \times 10^{-3}$ (the overbar here represents the averaged
 177 value of n_E calculated in the range $10^{-6} \leq k\eta \leq 10^{-2}$), which is around 0.3%.
 178 This value is sensibly smaller than the intermittency corrections usually re-
 179 ported in the literature for the energy spectrum, for which $E(k) \propto k^{-5/3-\mu/9}$,
 180 $\mu \in [0.1, 0.3]$.

181 Once the distribution of F is prescribed, the production term $Z(F) =$
 182 $Z(r, t)$ in (7) can be calculated exactly via the integral relation [35]:

$$Z(r, t) = 12r \int_0^\infty \left(\frac{1}{15} + \frac{\sin(kr)}{(kr)^3} + 3 \frac{\cos(kr)}{(kr)^4} - 3 \frac{\sin(kr)}{(kr)^5} \right) F(k) dk \quad (15)$$

183 Using equations (13), (14) and (15) the budget terms in (7) can be anal-
 184 ysed using the EDQNM data. This is shown in figure 3. Recall that $Z = 0$
 185 in decaying HIT while $\partial S_2/\partial t = 0$ for the statistically steady forced HIT.
 186 The values of S_3 calculated using (7), where each term on the right side
 187 of the equation are evaluated, and those using (14) are in good agreement;
 188 very small differences are observed for $r/\eta \approx 1$ which are due to the dis-
 189 cretization procedures used to calculate the derivatives of S_2 . As expected,
 190 the viscous term is dominant for $r/\eta \leq 5$ while the large-scale contributions

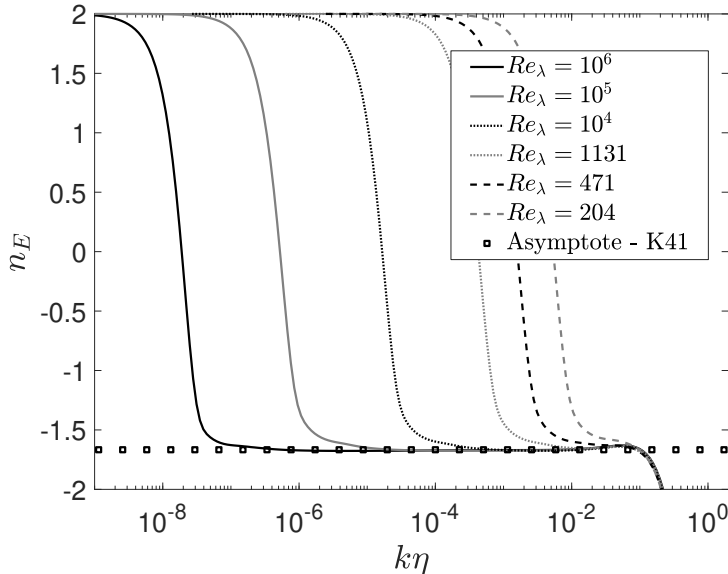


Figure 2: Local slope, $n_E(k)$, of the spectrum $E(k)$ for decaying HIT.

191 associated with Z or $\partial S_2/\partial t$ dominate at large r/η . Quite interestingly, the
 192 oscillatory tail behaviour exhibited by Z in figure 3(b) is also observed in
 193 the experimental data of forced turbulence by Moisy et al. [36]. Note that
 194 there is a small range of r where $Z/(\bar{\epsilon}r)$ exceeds 0.8; over this range, $S_3/(\bar{\epsilon}r)$
 195 must change sign in order to satisfy Equation 7. This effect is governed by
 196 the prescribed distribution of F . Note also that, at $Re_\lambda = 10^6$, $-S_3/(\bar{\epsilon}r)$ is
 197 approximately constant (≈ 0.8 within 0.1%) over not much more than one
 198 decade in r for decaying HIT compared with three decades for forced HIT.
 199 This clearly reflects the difference between the distributions of $-\frac{3}{r^4} \int_0^r s^4 \frac{\partial S_2}{\partial t} ds$
 200 and Z . These budget terms are never exactly zero in the scaling range, so
 201 that $-S_3/(\bar{\epsilon}r) = 0.8$ is never obtained for both decaying and forced HIT.
 202 For forced HIT, the scaling range, as a result of the particular choice of Z ,
 203 extends to values of r/L which exceed 0.1 (see Figure A.15 (b)).

204 3. Results

205 3.1. Energy Spectrum E and interscale energy flux Π

206 In this subsection the results obtained using the EDQNM model are
 207 validated via comparison with experimental and DNS data for moderate
 208 Re_λ . As opposed to structure functions, comparisons of energy spectra and
 209 non-linear energy transfer are much less common in the literature. First,
 210 the three-dimensional energy spectrum $E(k)$ and the interscale energy flux
 211 $\Pi(k) = \int_k^{+\infty} T(k) dk$ are considered. Comparisons with DNS results for both

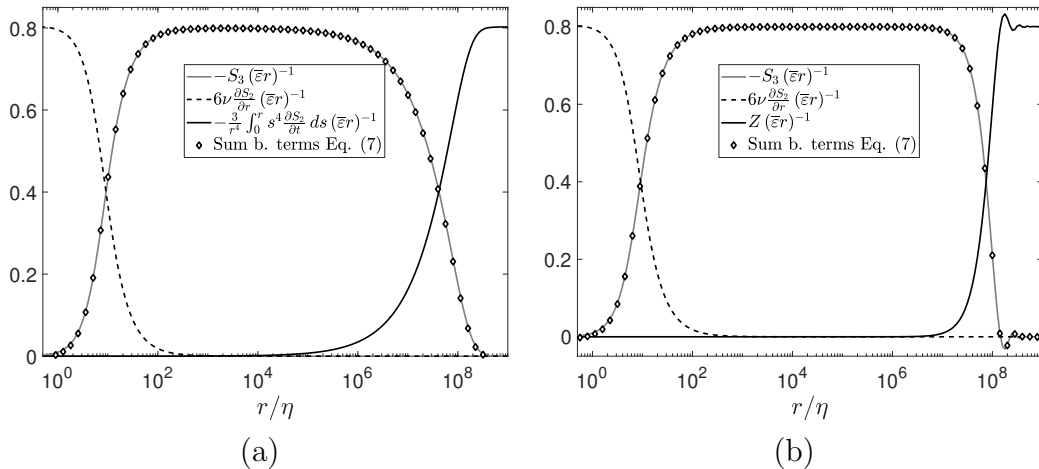


Figure 3: Budget terms (normalized by $(\bar{\epsilon}r)$) in Eq. 7 obtained from the EDQNM results for S_3 . Results are shown at $Re_\lambda = 10^6$ for (a) decaying HIT and (b) statistically steady forced HIT using the single wavenumber model in equation 9. Continuous black lines represent the terms (a) $-\frac{3}{r^4} \int_0^r s^4 \frac{\partial S_2}{\partial t} ds$ and (b) Z , respectively, while the dashed lines represent the viscous term $6\nu \frac{\partial S_2}{\partial r}$. Grey lines represent S_3 . White markers represent the sum of the normalized four budget terms of Eq. 7 i.e. $4/5 - (6\nu \frac{\partial}{\partial r} S_2(r) - \frac{3}{r^4} \int_0^r s^4 \frac{\partial S_2}{\partial t} ds + Z)(\bar{\epsilon}r)^{-1}$

212 forced HIT (Ishihara et al. [37]) and decaying free turbulence (Lamballais et
213 al. [38]) are shown in figure 4. Overall, a good agreement is observed. The
214 main differences are associated with the prediction of the bottleneck region
215 of three-dimensional energy spectra. A larger peak in the bottleneck region
216 is observed in the DNS distributions. This difference could be due to the
217 EDQNM modelling as well as to the DNS discretization error due to a lack
218 of small scale resolution. The difference between EDQNM and DNS results
219 appears to be more marked for the data of Ishihara et al, where a mesh res-
220 olution $k_{max}\eta \approx 1$ is employed. On the other hand, the data of Lamballais
221 et al. are obtained for $k_{max}\eta \approx 7.5$, which is much closer to the EDQNM
222 resolution ($k_{max}\eta > 10$). For the forced cases, a satisfactory agreement is
223 observed for the energy flux in figure 4(b) for $k\eta \geq 6 \times 10^{-3}$ and figure 4(d)
224 for $k\eta \geq 10^{-2}$. Similarly, the agreement for $-S_3/(\bar{\epsilon}r)$ shown in figure A.16(c)
225 seems adequate in the intermediate scale range. It is perhaps surprising that
226 EDQNM and DNS results show a good match for the quantities determined
227 by the non-linear energy transfer $T(k, t)$, which is the only modelled term
228 in the EDQNM. Once T is obtained, the calculation of E in the EDQNM
229 framework is virtually exact, as the energy spectrum is directly derived from
230 the Lin equation. Thus, the differences observed for the three-dimensional
231 energy spectrum in Figure 4(a)-(c) are most probably due to the forcing

232 schemes employed, which are different for DNS and EDQNM. For the forced
 233 cases, one can also see that the variation of the interscale energy flux Π is
 234 less abrupt for the multiscale forcing proposed in Equation 10. The large
 235 scale behaviour in this case is more similar to the DNS data by Ishihara et
 236 al. [37], which were also obtained using a large-scale forcing.

237 A quantitative measure of the discrepancy between a given spectrum E'
 238 and the reference spectrum E'' with which E' is compared is provided by the
 239 function

$$\mathcal{N}(E', E'') = \sqrt{\frac{\int_0^{+\infty} (E' - E'')^2 dk}{\int_0^{+\infty} (E'')^2 dk}} \quad (16)$$

240

241 For freely decaying HIT, the comparison of the EDQNM spectrum with
 242 results from Lamballais et al. [38] provides a discrepancy of $\mathcal{N}(E^{EDQNM}, E^{DNS}) =$
 243 0.1044 i.e. a global difference of $\approx 10\%$. The measure of the discrepancy for
 244 the EDQNM forced cases with the DNS data from Ishihara et al. is glob-
 245 ally much higher because of the differences observed at the large scales due
 246 to the different forcing employed as well as for the tails observed in the
 247 DNS at the small scales. However, if these two regions are excluded, the
 248 measured discrepancy is $\mathcal{N}(E^{EDQNM}, E^{DNS}) = 0.116$ for $Re_\lambda = 1131$ and
 249 $\mathcal{N}(E^{EDQNM}, E^{DNS}) = 0.1246$ for $Re_\lambda = 471$. The discrepancy is slightly
 250 higher for the lower Re_λ . This result is somehow expected considering that
 251 the EDQNM hypotheses should be better fulfilled for very high Re_λ , when a
 252 clear scale separation is obtained.

253 The EDQNM data are now compared with one-dimensional energy spec-
 254 tra measured in grid turbulence. The three-dimensional EDQNM spectra are
 255 manipulated to obtain the 1D spectra via the isotropic relation:

$$E_{11}(k_1) = \int_{k_1}^{+\infty} \frac{E(k)}{k} \left(1 - \frac{k_1^2}{k^2}\right) dk \quad (17)$$

256 The results for freely decaying HIT calculated via the EDQNM model are
 257 compared with the grid turbulence measurements of Mydlarski & Warhaft
 258 [39] in figure 5 for $Re_\lambda = 448, 199$. There is a reasonable agreement be-
 259 tween the shapes of the spectra. In particular, both the EDQNM and
 260 experimental compensated spectrum $E_{11}(k_1)/(\varepsilon_1^{-2/3} k_1^{-5/3})$ exhibit a maxi-
 261 mum at about $k_1 \eta_1 \simeq 0.05$. In this case, the measured discrepancy is
 262 $\mathcal{N}(E_{11}^{EDQNM}, E_{11}^{Exp}) = 0.092$ for $Re_\lambda = 448$ and $\mathcal{N}(E_{11}^{EDQNM}, E_{11}^{Exp}) = 0.1338$
 263 for $Re_\lambda = 199$, which is comparable to the discrepancy measured between
 264 DNS and EDQNM data. An adequate comparison is also obtained with
 265 the one dimensional energy spectra by Bodenschatz et al. [40] for $Re_\lambda =$

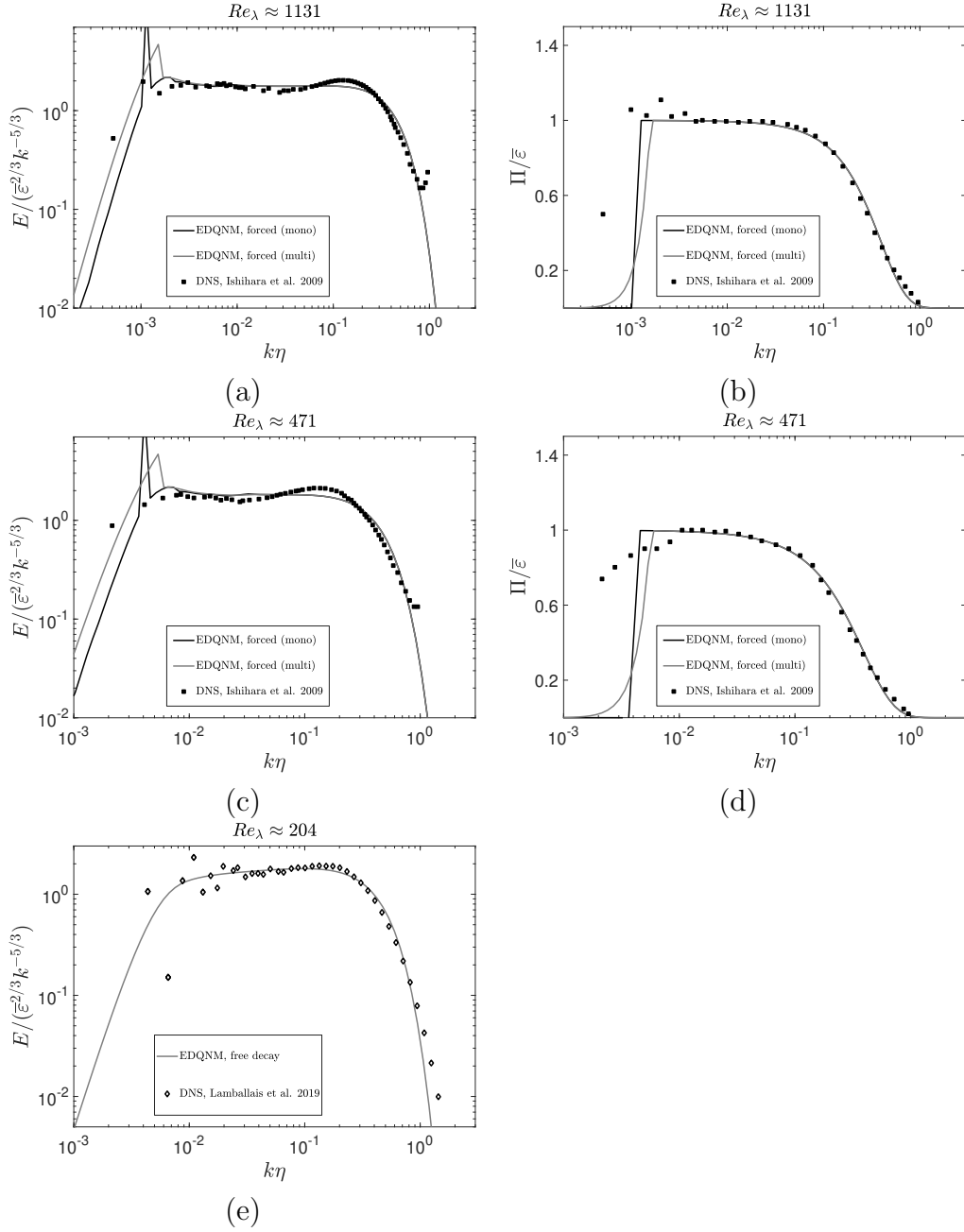


Figure 4: Comparison of EDQNM and DNS data for moderately high Re_λ . The compensated (left column) energy spectrum and (right column) energy flux are shown. DNS data are taken from Ishihara et al. [37] ((a) to (d)) and Lamballais et al. [38] (e).

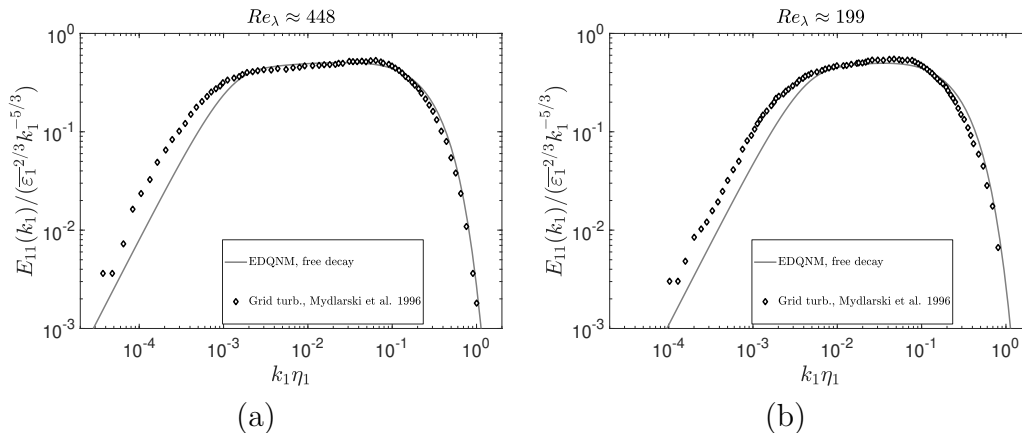


Figure 5: Comparison of EDQNM and grid turbulence results for low Re_λ . The compensated one-dimensional energy spectrum is shown. Grid turbulence data are taken from Mydlarski & Warhaft [39]

266 1370, 1620, as shown in Fig. 6. Here, the magnitude \mathcal{N} is larger, namely
 267 $\mathcal{N}(E_{11}^{EDQNM}, E_{11}^{Exp}) = 0.193$ for $Re_\lambda = 1620$ and $\mathcal{N}(E_{11}^{EDQNM}, E_{11}^{Exp}) = 0.195$
 268 for $Re_\lambda = 1370$. However, the value of \mathcal{N} for the two experimental spectra is
 269 $\mathcal{N}(E_{11}^{Exp(Re_\lambda=1370)}, E_{11}^{Exp(Re_\lambda=1620)}) = 0.08$ while a similar comparison between
 270 the EDQNM spectra provides a result of $\mathcal{N}(E_{11}^{EDQNM(Re_\lambda=1370)}, E_{11}^{EDQNM(Re_\lambda=1620)}) =$
 271 0.0049 , i.e. about 16 times smaller. The relatively high difference observed
 272 between the experimental spectra, which were obtained in the same wind
 273 tunnel but at slightly different values of Re_λ , suggests that the larger discrepancy
 274 between EDQNM and experiments for this case may be at least
 275 partially attributed to other reasons. Indeed, it is unrealistic to expect a
 276 perfect match between numerical and experimental results owing to the intrinsic
 277 differences in the way experiments are set up (and the associated
 278 uncertainties).

279 Further, EDQNM results are compared with one-dimensional spectra in
 280 the research work by Comte-Bellot & Corrsin [41] for $Re_\lambda \approx 65$. Results
 281 are shown in Figure 7 (a). The two spectra extracted from [41] shown in
 282 the figure were obtained for $U_0 t/M = 42, 171$ where U_0 is the asymptotic
 283 velocity, t is the time and M the mesh size (see Ref. [41] for a full description
 284 of the experimental set-up). These spectra are affected by noise,
 285 considering they have been calculated using the same acquisition system at
 286 similar Re_λ . The EDQNM data are consistent with the experimental spectra,
 287 in particular for $U_0 t/M = 171$. The measure of the discrepancy between
 288 the three spectra is comparable, i.e. $\mathcal{N}(E_{11}^{EDQNM}, E_{11}^{Exp(U_0 t/M=42)}) = 0.349$,
 289 $\mathcal{N}(E_{11}^{EDQNM}, E_{11}^{Exp(U_0 t/M=171)}) = 0.231$ and $\mathcal{N}(E_{11}^{Exp(U_0 t/M=42)}, E_{11}^{Exp(U_0 t/M=171)}) =$
 290 0.406 . Further, following the work by Cambon et al. [42] we performed a

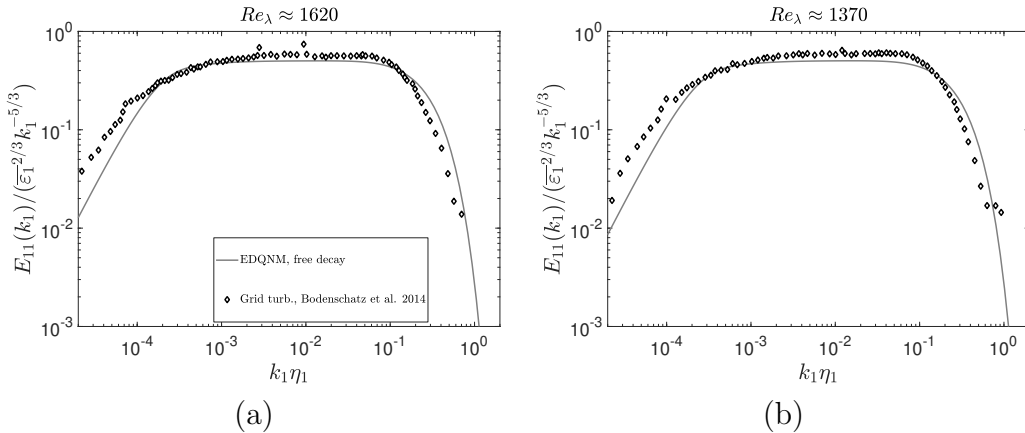


Figure 6: Comparison of EDQNM and grid turbulence results for moderate Re_λ . The compensated one-dimensional energy spectrum is shown. Grid turbulence data are taken from Bodenschatz et al. [40]

291 comparison of three-dimensional spectra. Comte-Bellot & Corrsin [41] pro-
 292 posed an analytic formula for $E(k)$ (which is the inverse of equation 17)
 293 to provide an estimation of the complete three-dimensional spectrum from
 294 measurements of E_{11} in HIT:

$$E(k) = \frac{1}{2} k^3 \frac{\partial}{\partial k} \left(\frac{1}{k} \frac{\partial}{\partial k} E_{11} \right) \quad (18)$$

295 The results reported by Comte-Bellot & Corrsin [41] are compared with
 296 the three-dimensional EDQNM spectrum in Figure 7 (b). One can see that
 297 in this case the comparison is not as good as for the one-dimensional spectra
 298 in Figure 7 (a). For $10^{-2} \leq k_1 \eta_1 \leq 1$, comparisons for compensated E_{11} and
 299 E provide similar indications. However, significant differences arise outside
 300 of this range. Equation 18 provides an over prediction of the density of
 301 turbulent kinetic energy at the large scales and an under prediction in the
 302 small scale region, which were not observed for E_{11} . These results are mainly
 303 due to the approximation in Equation 18.

304 The previous comparison at moderate Reynolds numbers highlights the
 305 capability of the EDQNM model to provide satisfactory predictions for $E(k, t)$
 306 and $T(k, t)$, which are the essential elements for the calculation of second
 307 and third order velocity structure functions. The principal advantage of the
 308 EDQNM model is that it can be performed at very high Reynolds regimes,
 309 currently unachievable with either experiments or DNS.

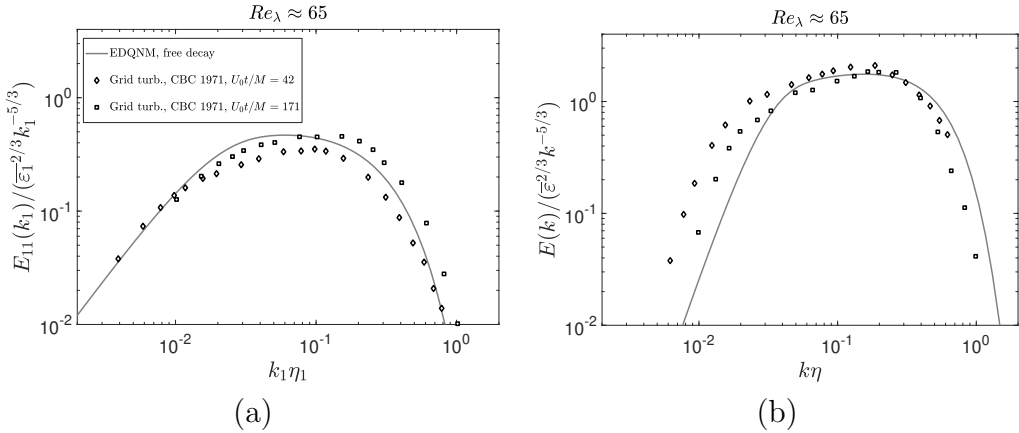


Figure 7: Comparison of EDQNM and grid turbulence results for moderate Re_λ . (a) The compensated one-dimensional energy spectrum and (b) the three-dimensional energy spectrum obtained via Eq. 18 are shown. Grid turbulence data are taken from Comte-Bellot & Corrsin [41]

3.2. Second-order structure function S_2

S_2 has been extensively studied over the last few decades. The scope of the present section is to provide a fairly extensive comparison between the present EDQNM results and those reported in the literature up to values of Re_λ not much larger than 10^3 . The Reynolds range covered by the EDQNM model is very large ($50 \leq Re_\lambda \leq 10^6$). This was possible because of the limited computational resources required by the model. Results for decaying and forced HIT are shown. For the latter, very minor variations were observed in the shapes of S_2 and S_3 for $r \approx L$ when using the two proposals for the forcing F . For this reason, results are here reported using the distribution of $F(k)$ in equation (9) only.

Results for the normalized distribution $S_2/(4\mathcal{K}/3)$ versus r/η are shown in figures 8(a) and 8(b) for both decaying and forced HITs, respectively. In both cases, one can see the emergence of three distinct regions with an increasing Re_λ ; they are, in order of increasing r/η , the dissipative range, the scaling range and the large-scale range. The shape and evolution of $S_2/(4\mathcal{K}/3)$ appear identical for both cases. To test if S_2 has a scaling range i.e. $(\bar{\epsilon}r)^{\zeta_2}$ with $\zeta_2 = 2/3$ we plot in Figures 8(c) and (d) $S_2/(\bar{\epsilon}r)^{2/3}$ versus r/η using a linear scale for the vertical axis. While both cases exhibit good collapse in the dissipative range ($r/\eta < 100$), the two cases differ substantially in the scaling range. In neither case can we identify a region where $S_2 \sim (\bar{\epsilon}r)^{2/3}$, which should have been marked by a plateau. The forced HIT, which shows a stronger departure from a plateau than the decaying HIT, exhibits a well defined bump in $S_2/(\bar{\epsilon}r)^{2/3}$ as the large scale region is approached.

334 Interestingly, the magnitude of this bump for the two largest values of Re_λ
 335 is the same, suggesting that it may have become independent of Re_λ . In the
 336 scaling range, the local slope $n_{S_2} = d\log(S_2)/d\log(\bar{\epsilon}r)$ continues to evolve
 337 with Re_λ although the possibility that it may eventually reach a constant for
 338 larger values of Re_λ than considered here cannot be excluded. The magnitude
 339 of n_{S_2} is shown in Figure 9. If a power law $S_2 \sim (\bar{\epsilon}r)^{n_{S_2}}$ exists, then n_{S_2} should
 340 be constant. The figure reveals that this is not strictly verified, so that the
 341 concept of a scaling range is at best only approximate. For $Re_\lambda = 10^6$ in
 342 both cases, n_{S_2} approaches a value of about 0.674 in the scaling range; 1%
 343 larger than $2/3$. This value is very close to that (0.679) obtained by McComb
 344 et al. [43] in forced HIT but smaller than that (0.72) found by Iyer et al. [44,
 345 45, 12] also in forced HIT. This discrepancy reflects the different approaches
 346 employed to estimate the power law exponent. In Iyer et al. [44, 45, 12] n_{S_2} is
 347 obtained via a global measure over almost two decades for r/L . The present
 348 values and those of McComb et al. [43] are instead estimated locally.

349 One can observe a difference in the way the constancy of n_{S_2} is approached
 350 for forced HIT (Figure 9 (b)). In decaying HIT, n_{S_2} decreases monotonically
 351 from 2 to 0 with increasing r . In forced HIT, n_{S_2} first decreases, then, at least
 352 for Re_λ larger than 471, increases slightly before decreasing to zero. This be-
 353 haviour, at least up to the largest Reynolds numbers investigated, prevents
 354 n_{S_2} to reach the same values as in decaying HIT in the scaling range. Similar
 355 observations have been reported by Lohse & Muller-Groeling [46]. Such a
 356 behaviour of n_{S_2} is associated with modified energy mode interactions which
 357 are responsible for an independent interscale energy flux from k in the scaling
 358 range, which leads to a steeper energy spectrum for $k > k_L$, discernible in
 359 Figure 1 (a) and which results in an energy pile-up. The intensity of this
 360 energy mode interactions is governed by the energy production mechanisms,
 361 represented here by $F(k)$. Further, the EDQNM results show that, for very
 362 large Reynolds number, while the energy pile up is restricted to the borders
 363 of the scaling range, it spreads over at least one decade in the spectral space.
 364 This can explain the apparent deviation from the $5/3$ law observed at moder-
 365 ate Re_λ . It is worth noting that the distribution of n_{S_2} is the same for both
 366 decaying and forced HITs in the range $0 \leq r/\eta \leq 10$, for all Re_λ , reflecting
 367 the universality of the dissipative range.

368 3.3. Third-order structure function S_3

369 The evolution of S_3 with the Reynolds number is reported in figure 10.
 370 The results are in agreement with previous results reported in the literature.
 371 In particular, the present results confirm the approach towards an establish-
 372 ment of the $4/5$ law as Re_λ continues to increase. Figure 11, which reports
 373 the variation of $C_3 = \max(-S_3/(\bar{\epsilon}r))$ with Re_λ , confirms the results of Qian

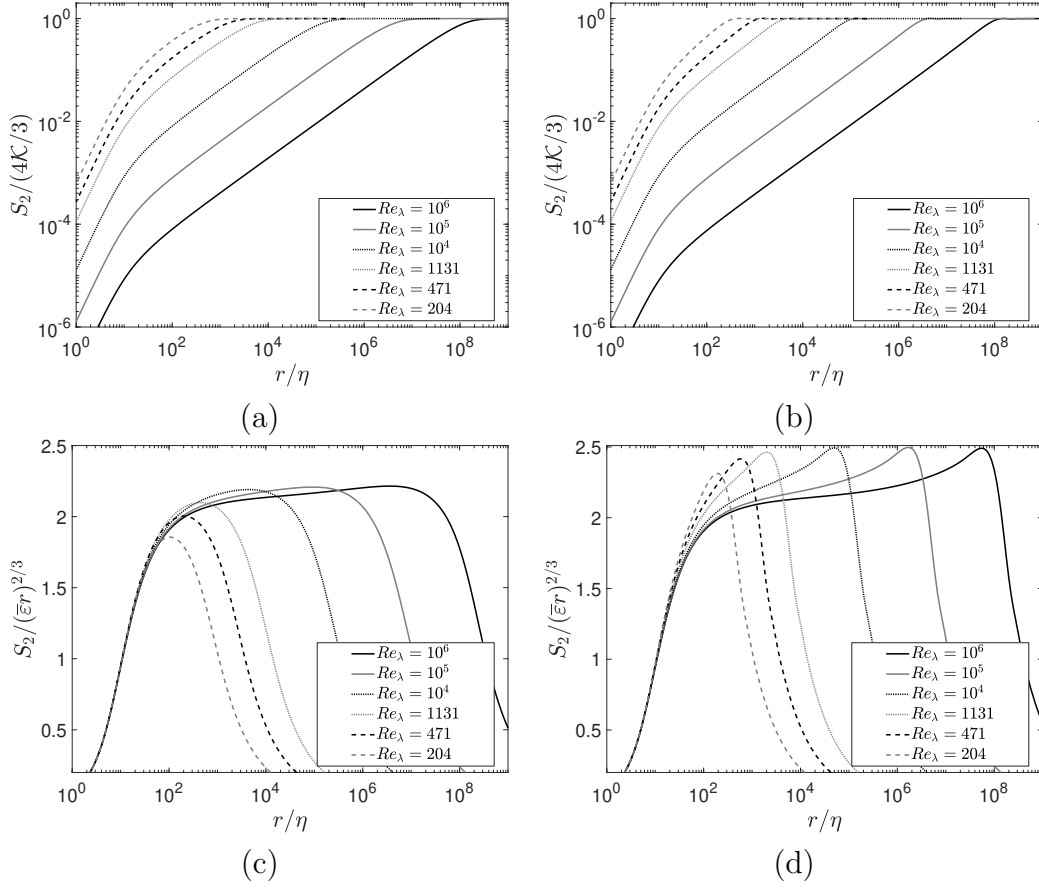


Figure 8: Structure function S_2 . (left column) free HIT decay and (right column) forced HIT obtained with EDQNM.

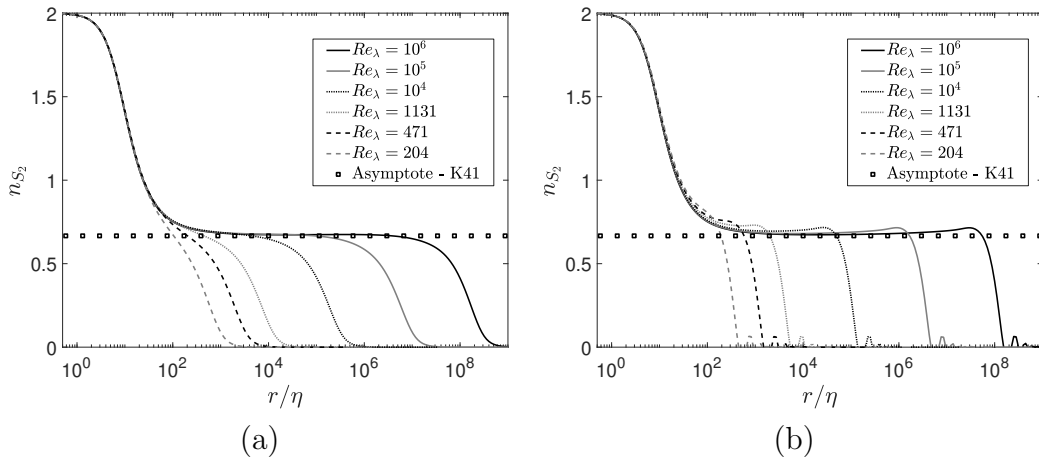


Figure 9: Local value of the slope, $n_{S_2}(r) \sim d \log(S_2)/d \log(\bar{\epsilon}r)$ for (a) decaying HIT and (b) forced HIT.

374 [8], Antonia & Burattini [9] and Tchoufag et al. [10]. While both cases ex-
 375 hibit a similar evolution, the value of Re_λ at which $C_3 \approx 0.8$ is first attained
 376 is, as expected, much lower for forced than for decaying HIT. The present
 377 results, which have been obtained by a single model run, match almost per-
 378 fectly the fit proposed by Antonia & Burattini [9]. On the other hand, the
 379 EDQNM results of Briard et al. (as reported in [23]) indicate higher values
 380 of C_3 , in particular for lower Reynolds numbers ($Re_\lambda < 10^2$). This difference
 381 is due to the different strategy used to obtain C_3 . Briard et al. performed a
 382 large number of simulations with initial spectra prescribed for several Re_λ .
 383 For each calculation, they sampled C_3 after 20 turn-over times, which may
 384 not be long enough to eliminate any lingering effects associated with the ini-
 385 tial conditions. This would support the idea that a departure from a pure
 386 free decay HIT would result in a larger C_3 yielding a larger rate at which
 387 the 4/5 law is reached with increasing Re_λ . It is also interesting to observe
 388 that the data by Briard et al. match pretty well C_3 values obtained from the
 389 reconstructed three-dimensional spectra from Comte-Bellot & Corrsin [41]
 390 and Cambon et al. [42]. As previously discussed, these spectra are affected
 391 by a significant noise and may exhibit as well a non-negligible departure
 392 from a freely decaying dynamic behaviour. Thus, one can expect that most
 393 flow configurations studied in realistic applications, where production and
 394 anisotropy effects cannot be completely eliminated, should fall in the area
 395 between the black line corresponding to the forced HIT prediction and the
 396 grey line representing the HIT free decay behaviour.

397 Finally, the variation of the slope $n_{S_3} = d\log(S_3)/d\log(\bar{\epsilon}r)$, is shown in
 398 figure 12. For both decaying and forced HIT, a linear dependence of S_3 on r
 399 emerges in the scaling range as Re_λ increases. There is a remarkable differ-
 400 ence between the behaviour of S_3 and S_2 in the scaling range when forcing
 401 is applied. Indeed, S_2 exhibits a noticeable bump at the upper end of the
 402 scaling range; such a bump is absent in S_3 . While this difference has yet
 403 to be explained, one can speculate that the bump observed in S_2 is linked
 404 to the energy spectrum which also exhibits a peak at the lower wavenum-
 405 bers. The product between the geometric function and E in the integrand
 406 of Eq. (13) exhibits very high values when r/η is in the wavenumber range
 407 corresponding to the forcing. This is consistent with the analysis by Lohse
 408 & Muller-Groeling [46]. On the other hand, the product between the geo-
 409 metric function and T in the integrand of Eq. (14) shows an oscillatory tail
 410 behaviour at larger values (almost by a factor of 3) of r/η , which are repre-
 411 sented in Figure 3(b). This can explain the difference in the scaling range
 412 behaviour between S_2 and S_3 .

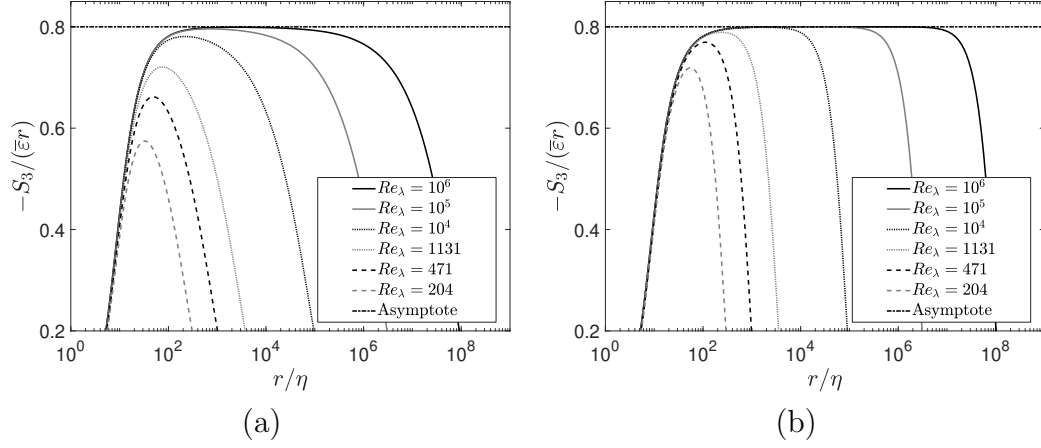


Figure 10: Structure function S_3 for (a) decaying and (b) forced HIT obtained with EDQNM.

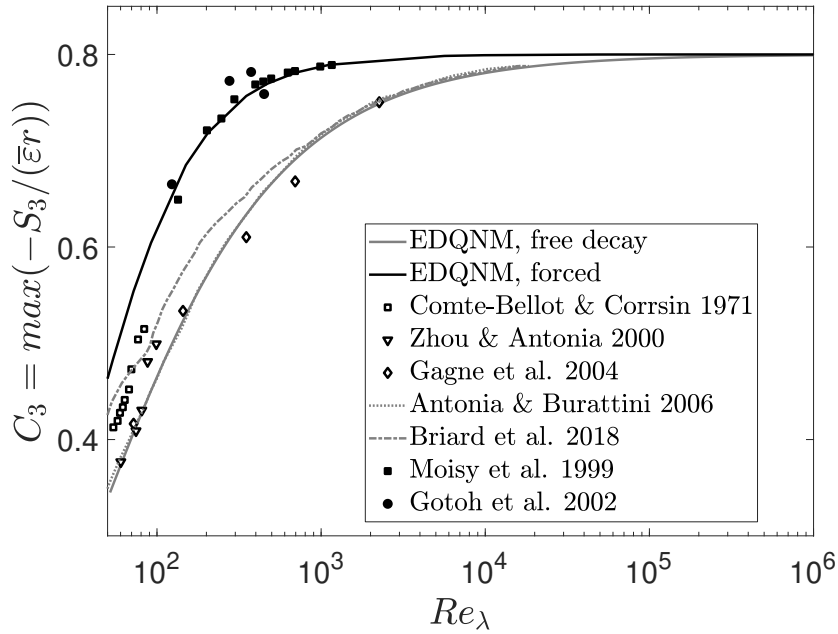


Figure 11: Maximum value C_3 for the normalized longitudinal structure function S_3 . Lines: present EDQNM; white symbols: reference data for HIT free decay; black symbols: reference data for forced HIT.

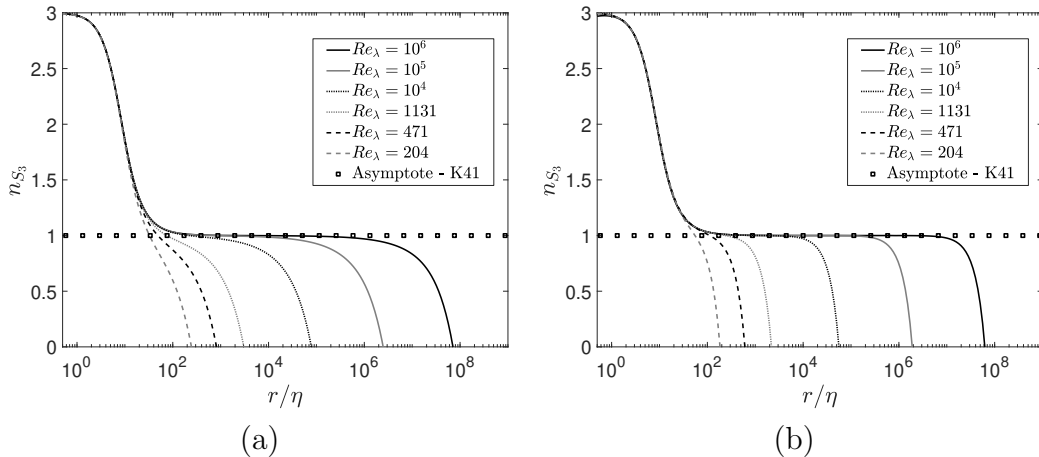


Figure 12: Local value of the slope, $n_{S_3}(r) \sim d \log(S_3)/d \log(\bar{\epsilon}r)$. (a): decaying HIT ;(b) forced HIT.

413 3.4. Skewness factor of the velocity increment, $S(r)$

414 We conclude this EDQNM analysis of S_2 and S_3 by presenting (Figure
415 13) the distributions of $S(r) = S_3/S_2^{3/2}$, the skewness factor of the velocity
416 increment δu for different Re_λ . Two interesting observations can be made.
417 Firstly, when $r \rightarrow 0$, $S(r)$ approaches a plateau with the same value in both
418 decaying HIT and forced HIT as Re_λ increases. As expected, the value of
419 $S(r \rightarrow 0)$ is practically identical to the velocity derivative skewness shown in
420 Figure A.14 in the appendix. Also both exhibit the same sensitivity to Re_λ .
421 Secondly, $S(r)$ shows a tendency to form a plateau in the scaling range when
422 Re_λ increases. One can expect that $S(r)$ may become constant in the scaling
423 range as Re_λ increases to infinitely large values. This behaviour seems to
424 conform with K41.

425 4. Conclusions

426 Numerical calculations, based on a EDQNM model, for both decaying
427 and forced HIT have been carried out with the aim of comparing the depend-
428 ence on the Reynolds number of second and third-order statistical moments
429 between the two cases. A recent EDQNM model [13] has been used, which
430 has yielded adequate matching with experimental and DNS data at low to
431 moderate Re_λ . The extensive validation of this matching suggests that the
432 extrapolation towards high Reynolds numbers should be reliable [or that at](#)
433 [least FRN effects identified via EDQNM should be comparable to those de-](#)
434 [scribed by the Navier-Stokes equations.](#) In fact, the 4/5 law remains a sine
435 qua non benchmark which can only be rigorously satisfied when Re_λ is very

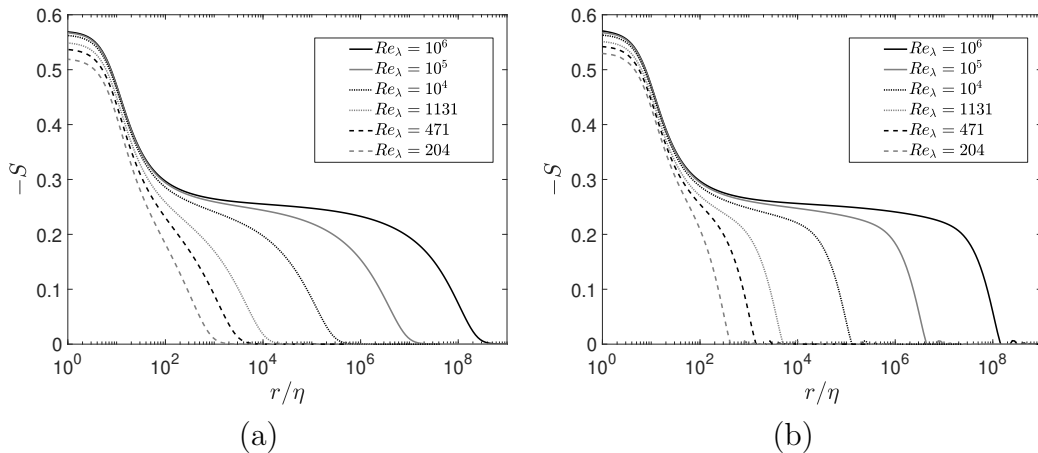


Figure 13: Skewness factor $S(r)$ of δu . EDQNM results for (left column) decaying HIT and (right column) forced HIT.

436 large. Since EDQNM captures the asymptotic 4/5 behavior as the Reynolds
 437 number increases (i.e. the second term, the third term and the fourth term
 438 of the right-hand side of equation 7 become negligible in the scaling range),
 439 its predictive capability at very large Re_λ should not be mistrusted. Also,
 440 the comparison between freely decaying and forced turbulence is performed
 441 using the same EDQNM model and, given that this model captures the differ-
 442 ence between these two types of turbulence at the maximum values of Re_λ
 443 currently possible in experimental or DNS data, there is no valid reason why
 444 the results from the model should not be meaningful at very high Reynolds
 445 numbers. The present EDQNM results are also in reasonable agreement with
 446 a recent extrapolation [11] based on an empirical model for S_2 . Particular
 447 attention has been given to the way S_2 and S_3 vary in freely decaying and
 448 forced HIT when the Reynolds number Re_λ increases to very large values, well
 449 beyond the reach of experiments and direct numerical simulations (DNSs).
 450 The results show that

- 451 1. reasonable agreement between EDQNM data and DNS / experimental
 452 results is observed, in the context of E and T , for moderate Re_λ . In
 453 particular, the compensated one-dimensional spectra E_{11} obtained from
 454 the EDQNM three-dimensional spectrum E is in reasonable agreement
 455 with grid turbulence results obtained by different authors.
- 456 2. the Kolmogorov normalized distributions of S_2 and S_3 in decaying and
 457 forced HIT collapse very well onto a single distribution in the dissipative
 458 range. This reinforces the analysis of Antonia et al. [47] and supports
 459 the argument that the dissipative range is likely to be unaffected by
 460 the large scales. The Kolmogorov-based similarity between decaying

461 and forced HIT distributions extends towards the scaling range as Re_λ
462 increases (see figure 1(e)-(f)). One expects that, with increasing Re_λ ,
463 the EDQNM distributions of S_2 and S_3 will asymptotically approach a
464 state which is consistent with the first similarity hypothesis of K41.

465 3. as Re_λ increases, S_3 reaches a reasonably convincing power-law be-
466 haviour over the scaling range, especially when forcing is applied. This
467 behaviour is fully consistent with the 4/5 law, Eq. 6, but it should
468 be emphasized that, with forcing, this behaviour extends to values of
469 r/L (see Figure A.15(b)) which approach 1 and is therefore difficult to
470 reconcile with the classical concept of an inertial range. Over the same
471 range, S_2 continues to evolve with Re_λ . For forced HIT, S_2 exhibits
472 a bump at the upper end of the scaling range where the forcing is in-
473 troduced. As Re_λ increases, and whilst the scaling range extends to
474 larger separations, the bump does not vanish, but its impact on smaller
475 separations decreases, paving the way towards a power-law behaviour.

476 The overriding conclusion that emerges from the present EDQNM results
477 is that, although S_3 exhibits a behaviour consistent with Eq. 6 when Re_λ
478 is sufficiently large, S_2 continues to evolve with Re_λ over the same range of
479 scales. While the EDQNM is not able to capture intermittency, the present
480 results suggest that observations of anomalous behaviors for n_{S_2} may not
481 only be due to intermittency effects, but to the interactions (possibly non-
482 linear) between several different aspects which include intermittency and
483 finite Reynolds number effects. If these observations are, in the future, con-
484 firmed by DNS for progressively higher Re_λ , this would raise some doubt
485 as to whether S_2 exhibits an anomalous scaling behaviour, as is usually re-
486 ported in the literature. This topic has also been recently discussed under the
487 perspective of Holder/Cauchy-Schwarz mathematical constraints [48]. The
488 present Re_λ trend in the scaling range does not exclude the possibility that,
489 irrespectively of whether the turbulence is decaying or forced, $S_2 \rightarrow (\overline{\varepsilon r})^{2/3}$
490 at even larger Reynolds numbers than considered here.

491 Also, it is difficult to discount the difference in the relative behavior of
492 S_2 and S_3 between decaying and forced HIT. This difference is evident in
493 experimental and DNS data and it is captured by the present EDQNM model.
494 The model shows that it persists when Re_λ is several orders of magnitude
495 larger than are currently achievable via experiment or DNS. An obvious
496 inference is that conclusions, e.g. with regard to the magnitudes of n_{S_2}
497 and n_{S_3} , drawn from forced turbulence studies do not necessarily apply to
498 decaying turbulence and vice versa.

499 Acknowledgements: Dr. C. Cambon and Dr. A. Briard are acknowledged
500 for fruitful discussion.

501 Competing interests: We declare we have no competing interests.

502 **References**

- 503 [1] T. Von Karman and L. Howarth. On the statistical theory of isotropic
504 turbulence. *Proceedings of the Royal Society A*, 164:192–215, 1938.
- 505 [2] A. N. Kolmogorov. Dissipation of energy in the locally isotropic tur-
506 bulence. *Dokl. Akad. Nauk SSSR*, 32 (see also Proc. R. Soc. Lond. A
507 (1991), 434, 15-17), 1941b.
- 508 [3] PG Saffman. Lectures on homogeneous turbulence. *Topics in nonlinear*
509 *physics*, pages 485–614, 1968.
- 510 [4] L. Danaila, F. Anselmet, T. Zhou, and R. A. Antonia. A generalization
511 of Yaglom’s equation which accounts for the large-scale forcing in heated
512 decaying turbulence. *J. Fluid Mech.*, 391:359–372, 1999.
- 513 [5] F. Thiesset, R. A. Antonia, and L. Djenidi. Consequences of self-
514 preservation on the axis of a turbulent round jet. *J. Fluid Mech.*,
515 748(R2), 2014.
- 516 [6] R.A. Antonia, S. L. Tang, L. Djenidi, and L. Danaila. Boundedness
517 of the velocity derivative skewness in various turbulent flows. *J. Fluid*
518 *Mech.*, 781:727–744, 2015.
- 519 [7] SL Tang, RA Antonia, L Djenidi, L Danaila, and Y Zhou. Finite
520 Reynolds number effect on the scaling range behaviour of turbulent
521 longitudinal velocity structure functions. *J. Fluid Mech.*, 820:341–369,
522 2017.
- 523 [8] J. Qian. Slow decay of the finite Reynolds number effect of turbulence.
524 *Physical Review E*, 60(3):3409, 1999.
- 525 [9] R.A. Antonia and P. Burattini. Approach to the 4/5 law in homogeneous
526 isotropic turbulence. *J. Fluid Mech.*, 550:175–184, 2006.
- 527 [10] J. Tchoufag, P. Sagaut, and C. Cambon. Spectral approach to finite
528 Reynolds number effects on Kolmogorov’s 4/5 law in isotropic turbu-
529 lence. *Phys. Fluids*, 24(1):015107, 2012.
- 530 [11] R.A. Antonia, S.L. Tang, L. Djenidi, and Y. Zhou. Finite Reynolds
531 number effect and the 4/5 law. *Physical Review Fluids*, 4:084602, 2019.

- 532 [12] K.P. Iyer, K.R. Sreenivasan, and P.K. Yeung. Scaling exponents satu-
533 rate in three-dimensional isotropic turbulence. *Physical Review Fluids*,
534 5:054605, 2020.
- 535 [13] W. J. T. Bos and J.-P. Bertoglio. Lagrangian Markovianized Field Ap-
536 proximation for turbulence. *J. Turb.*, 14(1):99, 2013.
- 537 [14] C. Cambon, N. N. Mansour, and F. S. Godeferd. Energy transfer in
538 rotating turbulence. *J. Fluid Mech.*, 337:303–332, 1997.
- 539 [15] W. J. T. Bos, H. Touil, and J.-P. Bertoglio. Reynolds number depen-
540 dency of the scalar flux spectrum in isotropic turbulence with a uniform
541 scalar gradient. *Phys. Fluids*, 17:125108, 2005.
- 542 [16] J Tchoufag, Pierre Sagaut, and Claude Cambon. Spectral approach to
543 finite Reynolds number effects on Kolmogorov’s 4/5 law in isotropic
544 turbulence. *Phys. Fluids*, 24(1):015107, 2012.
- 545 [17] M. Meldi and P. Sagaut. On non-self-similar regimes in homogeneous
546 isotropic turbulence decay. *J. Fluid Mech.*, 711:364–393, 2012.
- 547 [18] V. Mons, C. Cambon, and P. Sagaut. A spectral model for homogeneous
548 shear-driven anisotropic turbulence in terms of spherically averaged de-
549 scriptors. *J. Fluid Mech.*, 788:147–182, 2015.
- 550 [19] M. Meldi. The signature of initial production mechanisms in isotropic
551 turbulence decay. *Phys. Fluids*, 28:035105, 2016.
- 552 [20] A. Briard, T. Gomez, and C. Cambon. Spectral modelling for passive
553 scalar dynamics in homogeneous anisotropic turbulence. *J. Fluid Mech.*,
554 799:159–199, 2016.
- 555 [21] S. A. Orszag. Analytical theories of turbulence. *J. Fluid Mech.*, 41:363
556 – 386, 1970.
- 557 [22] M. Lesieur. *Turbulence in Fluids (4th edition)*. Springer, 2008.
- 558 [23] P. Sagaut and C. Cambon. *Homogenous Turbulence Dynamics*. Springer
559 Verlag, 2018.
- 560 [24] W. J. T. Bos and J.-P. Bertoglio. A single-time two-point closure based
561 on fluid particle displacements. *Phys. Fluids*, 18:031706, 2006.
- 562 [25] R. Kraichnan. Lagrangian-history closure approximation for turbulence.
563 *Physics of Fluids*, 8:575, 1965.

- 564 [26] M. Meldi and P. Sagaut. An adaptive numerical method for solving
565 EDQNM equations for the analysis of long-time decay of isotropic tur-
566 bulence. *Journal of Computational Physics*, 262:72–85, 2014.
- 567 [27] M. Meldi, H. Lejembre, and P. Sagaut. On the emergence of non-
568 classical decay regimes in multiscale/fractal generated isotropic turbu-
569 lence. *J. Fluid Mech.*, 756:816–843, 2014.
- 570 [28] S. Laizet, J. Nedic, and J. C. Vassilicos. The spatial origin of $-5/3$ spectra
571 in grid-generated turbulence. *Physics of Fluids*, 27:065115, 2015.
- 572 [29] G. Melina, P.J.K. Bruce, and J.C. Vassilicos. Vortex shedding effects in
573 grid-generated turbulence. *Physical Review Fluids*, 1:044402, 2016.
- 574 [30] S. B. Pope. *Turbulent Flows*. Cambridge University Press, 2000.
- 575 [31] J. Meyers and C. Meneveau. A functional form for the energy spec-
576 trum parametrizing bottleneck and intermittency effects. *Phys. Fluids*,
577 20(6):065109, 2008.
- 578 [32] G. Comte-Bellot and S. Corrsin. The use of a contraction to improve
579 the isotropy of grid-generated turbulence. *J. Fluid Mech.*, 25:657 – 682,
580 1966.
- 581 [33] W. J. T. Bos, L. Chevillard, J. F. Scott, and R. Rubinstein. Reynolds
582 number effect on the velocity increment skewness in isotropic turbulence.
583 *Phys. Fluids*, 24:015108, 2012.
- 584 [34] M. Meldi and P. Sagaut. Investigation of anomalous very fast decay
585 regimes in homogeneous isotropic turbulence. *J. Turb.*, 19:390–413,
586 2018.
- 587 [35] T. Gotoh, D. Fukayama, and T. Nakano. Velocity field statistics in
588 homogeneous steady turbulence obtained using a high-resolution direct
589 numerical simulation. *Physics of Fluids*, 14:1065, 2002.
- 590 [36] F. Moisy, P. Tabeling, and H. Willaime. Kolmogorov Equation in a Fully
591 Developed Turbulence Experiment. *Physical Review Letters*, 80:3994–
592 3997, 1999.
- 593 [37] T. Ishihara, T. Gotoh, and Y. Kaneda. Study of high Reynolds number
594 isotropic turbulence by Direct Numerical Simulation. *Annual Review of*
595 *Fluid Mechanics*, 41:165–180, 2009.

- 596 [38] E. Lamballais, T. Dairay, S. Laizet, and J.C. Vassilicos. Implicit/explicit
597 spectral viscosity and large-scale SGS effects. In *Direct and Large-Eddy*
598 *Simulation XI*, pages –. Springer, 2019.
- 599 [39] L. Mydlarski and Z. Warhaft. On the onset of high- Reynolds-number
600 grid-generated wind tunnel turbulence. *J. Fluid Mech.*, 320:331–368,
601 1996.
- 602 [40] E. Bodenschatz, G. P. Bewley, H. Nobach, M. Sinhuber, and H. Xu.
603 Variable density turbulence tunnel facility. *Review of Scientific Instru-*
604 *ments*, 85:093908, 2014.
- 605 [41] G. Comte-Bellot and S Corrsin. Simple eulerian time correlation of full
606 and narrow-band velocity signals in grid-generated, isotropic turbulence.
607 *J. Fluid Mech.*, 48:273–337, 1971.
- 608 [42] C. Cambon, D. Jeandel, and M. Mathieu. Spectral modelling of homo-
609 geneous non-isotropic turbulence. *J. Fluid Mech.*, 104:247–262, 1981.
- 610 [43] W. D. McComb, S. R. Yoffe, M. F. Linkmann, and A. Berera. Spec-
611 tral analysis of structure functions and their scaling exponents in forced
612 isotropic turbulence. *Physical Review E*, 90:053010, 2014.
- 613 [44] K.P. Iyer, K.R. Sreenivasan, and P.K. Yeung. Reynolds number scal-
614 ing of velocity increments in isotropic turbulence. *Physical Review E*,
615 95:021101, 2017.
- 616 [45] L. Biferale, F. Bonaccorso, M. Buzzicotti, and K.P. Iyer. Self-similar
617 subgrid-scale models for inertial range turbulence and accurate mea-
618 surements of intermittency. *Physical Review Letters*, 123:014503, 2019.
- 619 [46] D. Lohse and A. Muller-Groeling. Bottleneck effects in turbulence:
620 scaling phenomena in r versus p space. *Physical Review Letters*,
621 74:1747–1750, 1995.
- 622 [47] R. A. Antonia, L. Djenidi, and L. Danaila. Collapse of the turbulent
623 dissipation range on Kolmogorov scales. *Phys. Fluids*, 26:045105, 2014.
- 624 [48] Lyazid Djenidi, Robert A Antonia, and S. L. Tang. Mathematical con-
625 straints on the scaling exponents in the inertial range of fluid turbulence.
626 *Phys. Fluids*, 33:031703, 2021.
- 627 [49] D. W. Meyer and F. Saggini. Testing the markov hypothesis in fluid
628 flows. *Physical Review E*, 93:053103, 2016.

- 629 [50] A. Pouquet, M. Lesieur, J.-C. André, and C. Basdevant. Evolution
630 of high reynolds number two-dimensional turbulence. *J. Fluid Mech.*,
631 75:305–319, 1975.
- 632 [51] J.-C. André and M. Lesieur. Influence of helicity on the evolution of
633 isotropic turbulence at high reynolds number. *J. Fluid Mech.*, 81:187–
634 207, 1977.
- 635 [52] M. Meldi and P. Sagaut. Further insights into self-similarity and self-
636 preservation in freely decaying isotropic turbulence. *Journal of Turbu-*
637 *lence*, 14:24–53, 2013.
- 638 [53] Y. Gagne, B. Castaing, C. Baudet, and Y. Malecot. Reynolds de-
639 pendence of third-order velocity structure functions. *Phys. Fluids*,
640 16(2):482–485, 2004.

641 Appendix A. Numerical details about the EDQNM model

642 The EDQNM model [21, 22, 23] is a turbulence closure in spectral space.
643 The non-linear energy transfer T in equation 8 is obtained via two important
644 approximations:

- 645 • The fourth order cumulants, which represent the deviation of the ve-
646 locity derivative pdf from a Gaussian distribution, are approximated
647 using an eddy-damping term (eddy damping hypothesis)
- 648 • Time integration is simplified via a Markovianization procedure. [Marko-](#)
649 [vian processes have been extensively used for the analysis of a large](#)
650 [number of applications for turbulent flows \(see the review article by](#)
651 [Meyer and Saggini \[49\] and references therein\).](#) Its application within
652 the EDQNM formalism implies that local non-linear times are much
653 shorter than the large-eddy turnover time, which is strictly tied with
654 scale separation observed for very high Reynolds numbers

A closed expression for the non-linear energy transfer $T(k, t)$ is obtained via shell integration of radius k :

$$T_{EDQNM} = \int_{p+q=k} \Theta_{kpq} g E(q, t) [E(p, t) p k^2 - E(k, t) p^3] \frac{dpdq}{pq} \quad (\text{A.1})$$

where Θ_{kpq} is a characteristic time resulting from the Markovian approxima-
tion and g is a geometric function. In the present article, a recent proposal

by Bos & Bertoglio [13] is used to calculate the term Θ_{kpq} in equation A.1. In the classical EDQNM formulation [21, 22] the term is calculated as:

$$\Theta_{kpq}^{-1} = \eta_E(k, t) + \eta_E(p, t) + \eta_E(q, t), \quad (\text{A.2})$$

where η_E is the EDQNM damping factor. This last term is usually calculated following the proposal by Pouquet et al. [50]:

$$\eta_E(k, t) = A \sqrt{\int_0^k p^2 E(p, t) dp + \nu k^2}. \quad (\text{A.3})$$

655 The free coefficient $A \in [0.3, 0.5]$ is chosen to optimize the value for
 656 the constant C_K in the relation $E(k, t) = C_K \overline{\varepsilon^{2/3}} k^{-5/3}$ [51]. One of the
 657 major drawbacks of such a procedure is that it is not possible to derive an
 658 optimal value for which every HIT statistical quantity exhibits a behaviour
 659 in agreement with experiments and DNS in the literature. For this reason,
 660 the damping factor η_E is here calculated resolving an evolution equation for
 661 the velocity-displacement cross-correlation spectrum \mathcal{F}_{CC} [24]:

$$\left(\frac{\partial}{\partial t} + \nu k^2 \right) \mathcal{F}_{CC}(k, t) = \sum_{i=1}^8 T_i^F(k, t) + E(k, t) \quad (\text{A.4})$$

662 The terms T_i^F are calculated via integration in the spectral space, similarly
 663 to T_{EDQNM} in equation A.1:

$$T_1^F(k, t) = -\frac{1}{8} \int_{p+q=k} \Theta_{kpq}^F f_1(k, p, q) p^3 E(q, t) F(k, t) \frac{dpdq}{pq} \quad (\text{A.5})$$

$$T_2^F(k, t) = -\frac{1}{8} \int_{p+q=k} \Theta_{kpq}^F f_2(k, p, q) q^3 E(p, t) F(k, t) \frac{dpdq}{pq} \quad (\text{A.6})$$

$$T_3^F(k, t) = +\frac{1}{8} \int_{p+q=k} \Theta_{kpq}^F f_3(k, p, q) k^3 E(p, t) F(q, t) \frac{dpdq}{pq} \quad (\text{A.7})$$

$$T_4^F(k, t) = +\frac{1}{8} \int_{p+q=k} \Theta_{kpq}^F f_4(k, p, q) k^3 E(q, t) F(p, t) \frac{dpdq}{pq} \quad (\text{A.8})$$

$$T_5^F(k, t) = -\frac{1}{4} \int_{p+q=k} \Theta_{qpq}^F f_5(k, p, q) p^3 E(k, t) F(q, t) \frac{dpdq}{pq} \quad (\text{A.9})$$

$$T_6^F(k, t) = +\frac{1}{4} \int_{p+q=k} \Theta_{qpq}^F f_6(k, p, q) k^3 E(p, t) F(q, t) \frac{dpdq}{pq} \quad (\text{A.10})$$

$$T_7^F(k, t) = -\frac{1}{4} \int_{p+q=k} \Theta_{qpq}^F f_7(k, p, q) q^3 E(k, t) F(p, t) \frac{dpdq}{pq} \quad (\text{A.11})$$

$$T_8^F(k, t) = -\frac{1}{4} \int_{p+q=k} \Theta_{qpq}^F f_8(k, p, q) q^3 E(p, t) F(k, t) \frac{dpdq}{pq} \quad (\text{A.12})$$

664

665 where the terms f_i are geometrical functions and the spectral time scale
 666 Θ_{kppq}^F is defined as:

$$(\Theta_{kppq}^F)^{-1} = \eta_E^X(k, t) + \eta_E(p, t) + \eta_E(q, t), \quad (\text{A.13})$$

667

The algebraic relation between η_E and \mathcal{F}_{CC} is:

$$\eta_E(k, t) = E(k, t)/\mathcal{F}_{CC}(k, t) + \nu k^2. \quad (\text{A.14})$$

668

The term νk^2 in (A.14) was included in the earlier work by Bos &
 669 Bertoglio [24] but was then excluded in their most recent formulation [13].
 670 In the present work, it is employed after initial tests provided a more accu-
 671 rate prediction of numerous physical quantities. The term η_E^X in equation
 672 A.13 is instead set to zero. Comparison between the classical EDQNM and
 673 the present proposal (EDQNM-LMFA) [13] show that results for free decay
 674 regimes are in qualitative agreement, as shown in figure A.14 (a) for the
 675 velocity skewness S . The high-Reynolds number asymptotic limit for the
 676 velocity derivative skewness S is in the second case $S \approx -0.57$, which is
 677 approximately 7% smaller than the result ($S \approx -0.53$) obtained with the
 678 classical EDQNM version [52] or with that observed in the majority of ex-
 679 perimental data [6]. The results obtained with the EDQNM-LMFA model
 680 appear to be slightly more sensitive to FRN effects. This larger sensitiv-
 681 ity is associated with a slow convergence towards the expected behaviour
 682 $\mathcal{F}_{CC}(k, t) \propto k^{-7/3}$ in the inertial range, which is clearly observed only for
 683 $Re_\lambda > 10^7$ [15]. In addition, the EDQNM-LMFA model provides predictions
 684 for the structure functions S_2 and S_3 which are closer to experimental and
 685 DNS data for moderate Re_λ , as will be shown next. In figure A.14 (b) a
 686 comparison of the compensated structure function $S_2/(\bar{\epsilon}r)^{2/3}$ is shown at
 687 $Re_\lambda = 10^5$. One can see that the classical EDQNM prediction is not close to
 688 the expected maximum value $max(S_2/(\bar{\epsilon}r)^{2/3}) \geq 2$ which is usually observed
 689 using high precision tools such as DNS.

690

A comprehensive preliminary analysis of second and third-order structure
 691 functions has been performed. First, EDQNM results for freely decaying
 692 and forced HIT are presented in Figure A.15. The terms $-\frac{3}{r^4} \int_0^r s^4 \frac{\partial S_2}{\partial t} ds$
 693 (freely decaying HIT) and Z (forced HIT) of Equation 7 provide very different
 694 contributions in the large scale region for $r/L \approx 1$ for S_3 in Figure A.15
 695 (b). In particular, $-S_3/(\bar{\epsilon}r)$ is approximately equal to 0.8 for values of r/L
 696 extending well beyond 0.1 for forced HIT. Also, $-S_3/(\bar{\epsilon}r)$ changes sign for
 697 $r/L \approx 3$, which is not far from the wavelength at which forcing is applied
 698 ($kL = 1$). Results for S_2 and S_3 using the EDQNM-LMFA method are

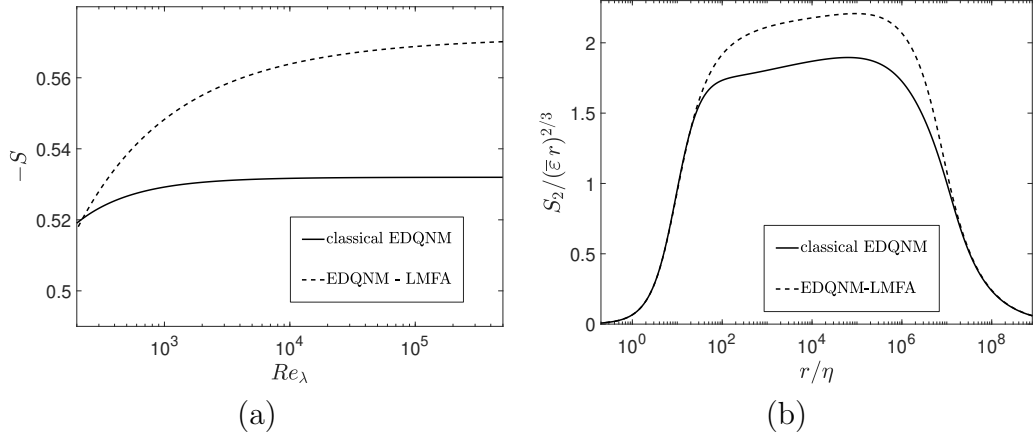


Figure A.14: Comparison of results obtained using the classical version of the EDQNM and the recent EDQNM-LMFA proposal for freely decaying HIT. (a) Velocity derivative flatness S behaviour in the range $Re_\lambda \in [200, 5 \times 10^5]$. (b) Compensated structure function $S_2/(\bar{\epsilon} r)^{2/3}$ for $Re_\lambda = 10^5$.

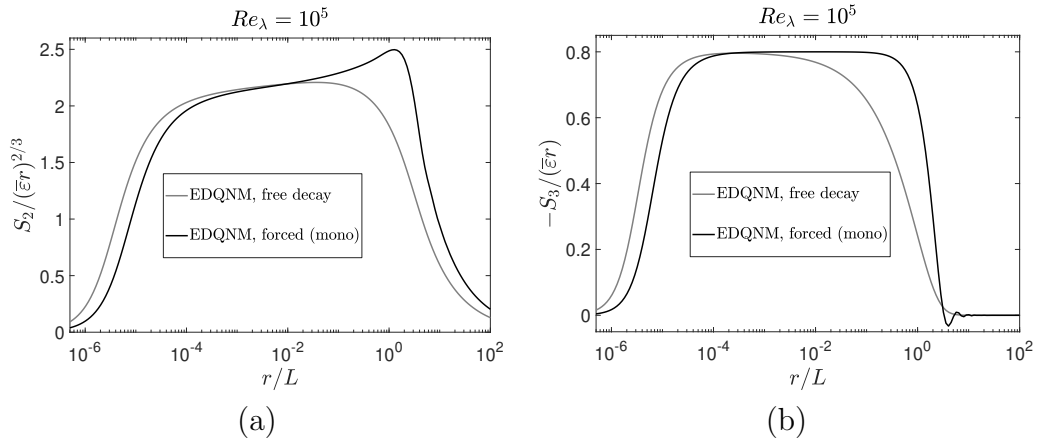


Figure A.15: Comparison between results for decaying and forced HIT of (a) the second-order structure function S_2 and (b) the third-order structure function S_3 at $Re_\lambda = 10^5$.

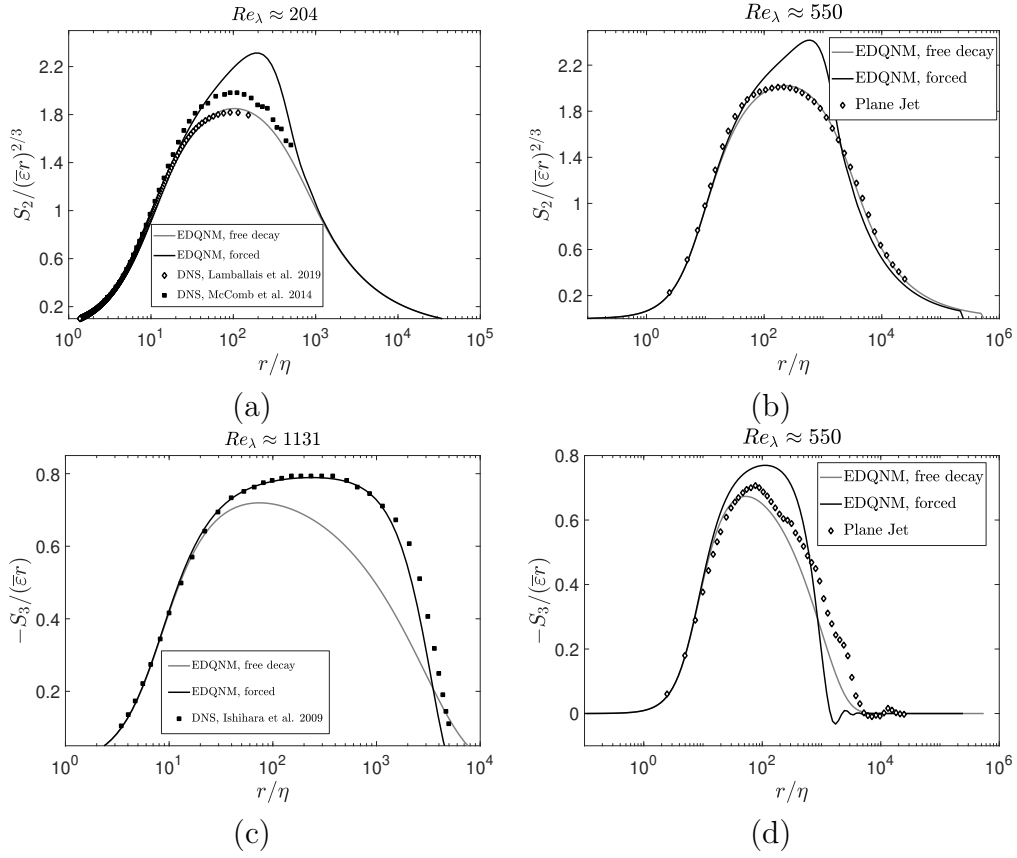


Figure A.16: EDQNM prediction for S_2 and S_3 . Comparisons are shown for: (a) S_2 with DNS data of forced HIT (McComb et al. [43]) and decaying HIT (Lamballais et al. [38]) for $Re_\lambda \approx 204$, (b) S_2 with experimental data for a plane jet for $Re_\lambda = 550$, (c) for S_3 with DNS data of forced HIT for $Re_\lambda = 1131$ and (d) for S_3 with experimental plane jet data [53] for $Re_\lambda = 550$.

699 compared in Figure A.16 with DNS / experimental results in the literature
700 [53, 37, 43, 38]. The agreement is generally adequate.